Anisotropic exchange within decoupled tetrahedra in the quantum breathing pyrochlore $Ba_3Yb_2Zn_5O_{11}$*

J. G. Rau,[1,†] L. S. Wu,[2,‡] A. F. May,[3] L. Poudel,[2,4] B. Winn,[2] V. O. Garlea,[2] A. Huq,[5] P. Whitfield,[5] A. E. Taylor,[2] M. D. Lumsden,[2] M. J. P. Gingras,[1,6,7] and A. D. Christianson[2,4]

[1]*Department of Physics and Astronomy, University of Waterloo, Ontario, N2L 3G1, Canada*
[2]*Quantum Condensed Matter Division, Oak Ridge National Laboratory, Oak Ridge, TN-37831, USA*
[3]*Materials Science & Technology Division, Oak Ridge National Laboratory, Oak Ridge, TN-37831, USA*
[4]*Department of Physics & Astronomy, University of Tennessee, Knoxville, TN-37966, USA*
[5]*Chemical & Engineering Materials Division, Oak Ridge National Laboratory, Oak Ridge, TN 37831, USA*
[6]*Perimeter Institute for Theoretical Physics, Waterloo, Ontario, N2L 2Y5, Canada*
[7]*Canadian Institute for Advanced Research, 180 Dundas Street West, Suite 1400, Toronto, ON, M5G 1Z8, Canada*

(Dated: February 19, 2022)

The low energy spin excitation spectrum of the breathing pyrochlore $Ba_3Yb_2Zn_5O_{11}$ has been investigated with inelastic neutron scattering. Several nearly resolution limited modes with no observable dispersion are observed at 250 mK while, at elevated temperatures, transitions between excited levels become visible. To gain deeper insight, a theoretical model of isolated Yb^{3+} tetrahedra parametrized by four anisotropic exchange constants is constructed. The model reproduces the inelastic neutron scattering data, specific heat, and magnetic susceptibility with high fidelity. The fitted exchange parameters reveal a Heisenberg antiferromagnet with a very large Dzyaloshinskii-Moriya interaction. Using this model, we predict the appearance of an unusual octupolar paramagnet at low temperatures and speculate on the development of inter-tetrahedron correlations.

Frustrated or competing interactions have been repeatedly found to be at the root of many unusual phenomena in condensed matter physics [1–5]. By destabilizing conventional long-range order down to low temperature, frustration in magnetic systems can lead to many exotic phases; from unconventional multipolar [6, 7] and valence bond solid orders [1, 4] to disordered phases such as classical and quantum spin liquids [1, 4]. Significant attention has been devoted to understanding *geometric* frustration where it is the connectivity of the lattice that hinders the formation of order. Recently, however, magnets frustrated not by geometry but by competing interactions have become prominent for the novel behaviors that they host. Such competing interactions might be additional isotropic exchange acting beyond nearest neighbors [8–10], biquadratic or other multipolar interactions [11]. One possibility attracting ever increasing interest is that competing strongly *anisotropic* interactions may stabilize a wide range of unusual phenomena.

An exciting research direction in the latter context concerns itself with so-called "quantum spin ice" [12]. This quantum spin liquid can be stabilized by perturbing classical spin ice with additional anisotropic transverse exchange interactions that induce quantum fluctuations. Particularly interesting is the potential realization of such physics in the rare-earth pyrochlores $R_2M_2O_7$ [13–15], where R is a trivalent $4f$ rare-earth ion, and M is a non-magnetic tetravalent transition metal ion, such as M=Ti, Sn or Zr. These materials can be described in terms of pseudo spin-1/2 degrees of freedom interacting via anisotropic exchanges [12, 15], where the effective spin-1/2 maps the states of the crystal-electric field ground doublet of the rare-earth ion. These materials display a wealth of interesting phenomena, from the possibility of quantum [16–18] order-by-disorder physics in $Er_2Ti_2O_7$ [19], unconventional ordered states [20, 21] as well as several candidates for quantum spin liquids [22, 23]. In many of these compounds, the physics is very delicate, showing strong sample to sample variations [24] or sensitivity to very small amounts of disorder [25, 26]. Consequently, an accurate determination of the effective model is crucial in making definite progress in this area. This is particularly true in cases where the idealized disorder-free material may find itself in the vicinity of a transition between competing semi-classical ground states [18, 27, 28]

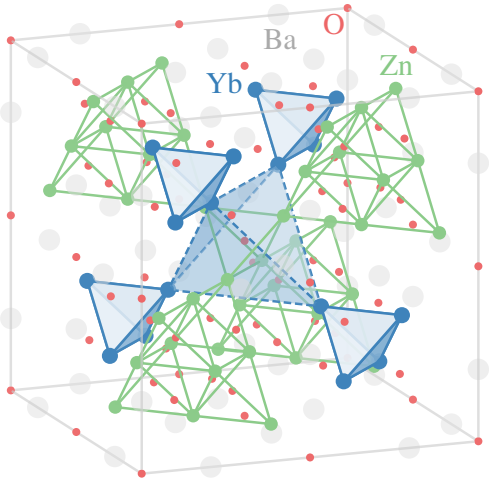

FIG. 1. Crystal structure of $Ba_3Yb_2Zn_5O_{11}$ (cubic space group $F\bar{4}3m$, no. 216). Each Yb^{3+} ion is part of a large and small tetrahedron in the breathing pyrochlore lattice.

Given the critical importance played by the precise value of the anisotropic exchanges, a number of experiments have been aimed at determining those couplings [15, 16]. There is, unfortunately, much difficulty in obtaining accurate values for these couplings stemming from two key limitations. First, only approximate methods are available to relate the model to ex-

periment, restricting comparisons to regimes where the theory becomes controlled, such as in high magnetic field [15, 16, 29] or at high-temperature [29–32]. Second, to avoid over-fitting the experimental data, one must work with a reasonable number of fitting parameters; for example restricting to a subset of the allowed interactions by ignoring interactions beyond nearest neighbors or possible multi-spin interactions [19]. Even in $Yb_2Ti_2O_7$, where the latter concern is largely absent, there currently remains no consensus on the values of the anisotropic exchange parameters [15, 27]. At the present time, a reference rare-earth pyrochlore-like compound with solely bilinear anisotropic interactions and for which essentially exact methods can be employed to compare with experimental data, is badly needed to cement the validity of the effective spin-1/2 description of such materials.

In this Letter, we study $Ba_3Yb_2Zn_5O_{11}$ (BYZO), a so-called breathing pyrochlore (BP) compound [33, 34], which provides an ideal platform for understanding such anisotropic exchange models. As shown in Fig. 1, BYZO consists of small tetrahedra with a short nearest-neighbor bond distance $r_< \sim 3$Å connected by large tetrahedra with size $r_> \sim 6$Å. Because of the large ratio $r_>/r_< \sim 2$, the inter-tetrahedron couplings are expected to be small compared to the intra-tetrahedron couplings, leading to effectively decoupled small tetrahedra. This can be compared to the Cr-based BP compounds, where the small and large tetrahedra only differ in size by $\sim 5\%$ [35–37]. To characterize BYZO spectroscopically, we have investigated its low energy spin excitations using inelastic neutron scattering (INS). We confirm the picture of nearly independent tetrahedra, seeing nearly resolution limited dispersion-less modes at low temperatures. This INS data, combined with the thermodynamic measurements of Ref. [33], allows for a complete and unambiguous determination of the the effective model for BYZO. We find that a single tetrahedron pseudo-spin model can quantitatively account for all of the current experimental data on BYZO, determining the four anisotropic exchanges as well as the g-tensor. In addition to the antiferromagnetic Heisenberg exchange postulated in Ref. [33], we find that significant Dzyaloshinskii-Moriya (DM) exchange is needed to obtain the correct level structure determined from INS. The fitted exchange parameters are far from the spin ice limit recently considered in Ref. [38] or the purely Heisenberg limits studied in Ref. [39]. Instead, we find the ground state of each tetrahedron is doubly degenerate, consistent with the residual entropy observed experimentally at $T \sim 300$ mK [33]. These E-doublets are nearly non-magnetic, carrying both a scalar spin-chirality as well as octupolar, all-in/all-out moments. The state of BYZO at currently studied base temperatures is thus a type of "octupolar paramagnet" without significant inter-tetrahedron correlations. Notwithstanding the broad agenda of accurately determining the anisotropic exchanges in rare-earth pyrochlore materials, the complete characterization of the single-tetrahedron model should provide a useful guide for further experimental studies of BYZO and other BPs. Specifically, we estimate that the inter-tetrahedron correlations could begin to set in below 500 mK, at the edge of currently explored temperatures, possibly leading to interesting new physics [40–44] in this material.

Experimental results: Polycrystalline samples of BYZO were synthesized by solid-state reaction in Al_2O_3 crucibles [45]. The resulting samples were characterized by specific heat and magnetization measurements [45]. The structure was studied via neutron powder diffraction utilizing the POWGEN [47] diffractometer at the Spallation Neutron Source at Oak Ridge National Laboratory [45]. These measurements confirm the previously reported cubic structure [33, 48, 49] (space group $F\bar{4}3m$, no. 216) with lattice parameter a=13.47117(3) at 10 K and a=13.48997(3) at 300 K.

To explore the low energy spectrum of magnetic excitations in BYZO, INS data was collected using the HYSPEC spectrometer [50] at the Spallation Neutron Source at Oak Ridge National Laboratory. Measurements were performed at 0.25, 10, and 20 K utilizing a ^{3}He refrigerator, with fixed incident neutron energies of $E_i = 3.8$ meV, 7.5 meV and 15 meV.

INS measurements with $E_i = 3.8$ meV at 0.25 and 20 K are shown in Fig. 2. The data at 0.25 K (Fig. 2(a) and (b)) exhibits several well-defined modes with no observable dispersion. The $|\mathbf{Q}|$-dependence of the inelastic scattering intensity exhibits a broad peak centered near $|\mathbf{Q}| = 1.3$Å^{-1} (see Fig. 2(b) and the Supplemental Material [45]). The width in energy of the modes is close to instrumental resolution [45]. At elevated temperatures (Fig. 2(b) and (d)), three new excitations become visible resulting from transitions between excited states.

The origin of the observed low energy excitations appears to be modes originating from *decoupled* Yb tetrahedra. Several pieces of evidence support this assertion. Low lying crystal field levels can be excluded as the origin of these modes as three higher energy crystal field levels are experimentally observed (the maximum number for Yb^{3+}) with the lowest lying level at ~ 38 meV [34, 45]. The magnetic susceptibility and specific heat data do not show any signs of long range magnetic order down to 0.38 K [33, 45] that would indicate correlations between the small tetrahedra. Examination of the elastic scattering at 0.25 K is consistent with this conclusion, revealing no indication of long range magnetic order. Finally, the lack of dispersion suggests that these modes arise primarily from isolated tetrahedra and that the interactions connecting the tetrahedra are weak. We note that there is a weak and broad feature at ~ 1 meV. We have been unable to identify the origin of this feature, but note that it has a $|\mathbf{Q}|$-dependence [45] distinct from that of the other nearly resolution limited modes.

Theoretical model: We now use these experimental observations, along with the thermodynamic data from Ref. [33] to construct a model of BYZO. Given the dispersion-less modes seen in the INS, and the large ratio $r_>/r_< \sim 2$ between the large and small tetrahedron sizes, we expect isolated Yb_4 tetrahedra to provide a very good description of the low energy physics. Each of the four Yb^{3+} ions has a Hund's rule ground state of $^2F_{7/2}$, with the $J = 7/2$ manifold strongly split by the C_{3v} ($3m$) crystalline electric field environment. Since this energy scale is very large, ~ 38 meV [34], relative to the expected scale of the intra-tetrahedron interactions, only the ground doublet is

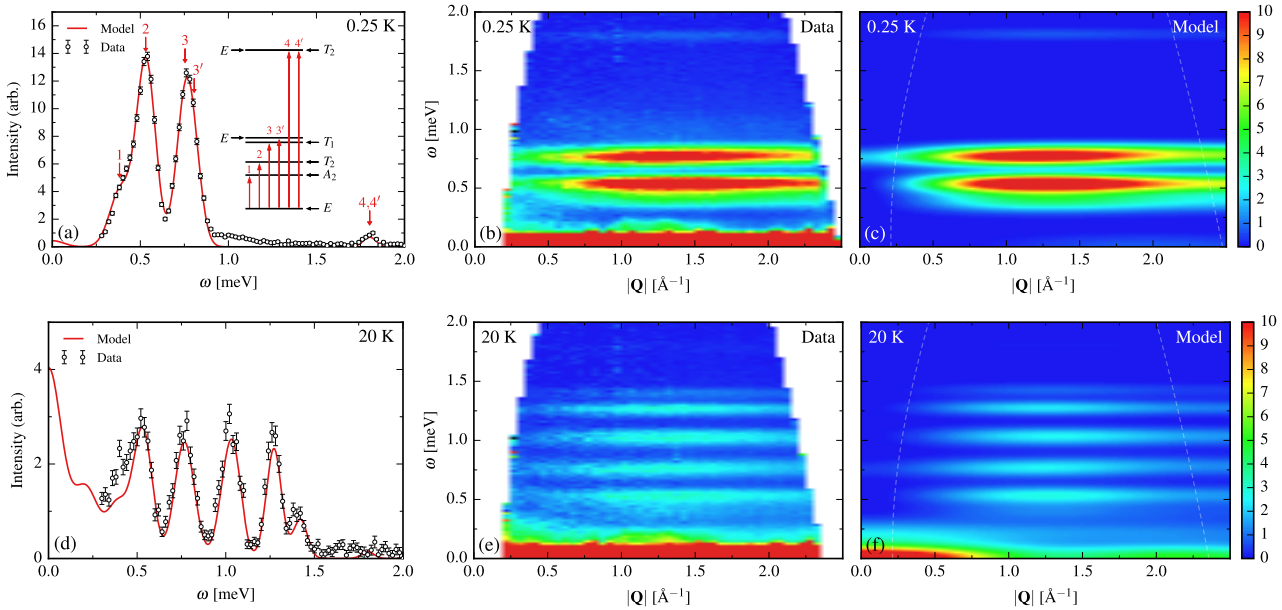

FIG. 2. INS data (E_i = 3.8 meV) and comparison to our theoretical model at (a-c) 0.25 K and (d-f) 20 K. The overall theoretical intensity scale was fit using the constant wavevector cut (a) at 0.25 K. A Gaussian broadening with energy dependence following the experimental energy resolution function [45] was included in the theoretical calculation. (a,d) Cut of the INS data averaged over the window 1.25Å^{-1} < |**Q**| < 1.35Å^{-1} at (a) 0.25 K and (b) 20 K. Results for model of Eq. (2) with fitted parameters of Eq. (3) are also shown. (Inset,a) An illustration of the level structure of the single-tetrahedron model and the positions of the transitions from the ground doublet into the excited states. (b,e) Intensity map of the powder averaged INS data at (c) 0.25 K and (d) 20 K. The excitations are nearly dispersion free over the full |**Q**| range. (c,f) Model calculations for the parameters of Eq. (3) are shown at (e) 0.25 K and (f) 20 K. The Yb^{3+} form factor was evaluated in the dipole approximation, as given in Ref. [46].

relevant at low temperatures. The two states of this doublet define an effective pseudo-spin $\mathbf{S}_i$ at each of the four Yb^{3+} sites. This pseudo-spin is related to the magnetic moment $\boldsymbol{\mu}_i$ at each site through the g-factors, g_z and $g_\pm$, present due to the local C_{3v} symmetry. Explicitly,

$$\boldsymbol{\mu}_i \equiv \mu_B \left[g_\pm \left(\hat{\mathbf{x}}_i S_i^x + \hat{\mathbf{y}}_i S_i^y \right) + g_z \hat{\mathbf{z}}_i S_i^z \right], \qquad (1)$$

where $(\hat{\mathbf{x}}_i, \hat{\mathbf{y}}_i, \hat{\mathbf{z}}_i)$ are the local axes of tetrahedron site i [45]. Regardless of the detailed composition of the ground doublet, since $J = 7/2$, the interactions between the Yb^{3+} are expected to be anisotropic and, a priori, not necessarily near the Ising or the Heisenberg limit [51]. Symmetry strongly constrains their form; each Yb^{3+}-Yb^{3+} bond has symmetry C_{2v} ($2mm$) and each small Yb_4 tetrahedron has full tetrahedral symmetry T_d ($\bar{4}3m$) [33, 49]. Assuming an effective spin-1/2 doublet [52], there are therefore four allowed anisotropic exchange interactions [15], taking the form

$$H_{\text{eff}} \equiv \sum_{i=1}^{4} \sum_{j<i} \left[J_{zz} S_i^z S_j^z - J_\pm \left(S_i^+ S_j^- + S_i^- S_j^+ \right) + J_{\pm\pm} \left(\gamma_{ij} S_i^+ S_j^+ + \text{h.c.} \right) + J_{z\pm} \left(\zeta_{ij} \left[S_i^z S_j^+ + S_i^+ S_j^z \right] + \text{h.c.} \right) \right], \qquad (2)$$

where the bond dependent phases γ_{ij} and ζ_{ij} are defined in the Supplemental Material [45]. The spectrum of this Hamiltonian is partly determined by tetrahedral symmetry. The four-pseudo-spin states break into the irreducible representations $A_2 \oplus 3E \oplus T_1 \oplus 2T_2$ under the action of the tetrahedral group. This gives a level structure of a singlet (A_2), three doublets (E) and three triplets (T_1 or T_2). From the observed residual entropy [33], it seems plausible that the ground state of the tetrahedron is an E doublet, which gives an entropy of $k_B \ln(2)/4 \sim 0.1733 k_B$ / Yb^{3+}.

Best fit parameters: The model of Eq. (2), supplemented with the definition of the moment in Eq. (1), is determined by the six parameters J_{zz}, $J_\pm$, $J_{\pm\pm}$, $J_{z\pm}$, g_z and $g_\pm$. To fix these parameters, we perform a fit to the specific heat and susceptibility data of Ref. [33] and a cut of the INS data averaged over the range 1.25Å^{-1} < |**Q**| < 1.35Å^{-1} at 0.25 K. This is a global fit, minimizing squared differences between experimental and theoretical values from each set of experimental data simultaneously. For the specific heat, we fit only the data below 5 K to minimize the influence of the subtraction of the lattice contribution, while the susceptibility data up to 30 K is used. [53]. Three additional fitting parameters were included; a constant shift of the susceptibility, χ_0, to account for the Van Vleck and diamagnetic core contributions of the Yb^{3+} ions, the intensity scale of the INS cut and the overall scale of the Gaussian broadening used in the theoretical INS intensity [45]. Further details

of the fitting methodology and comparisons to experimental data can be found in the Supplemental Material [45].

From this analysis we find a unique best fit which provides excellent agreement with *all* of the known experimental data on BYZO. The best fit parameters are

$$\begin{aligned} J_{zz} &= -0.037 \text{ meV}, & J_{\pm} &= +0.141 \text{ meV}, \\ J_{\pm\pm} &= +0.158 \text{ meV}, & J_{z\pm} &= +0.298 \text{ meV}, \\ g_{\pm} &= 2.36, & g_z &= 3.07. \end{aligned} \tag{3}$$

Comparison to the specific heat and susceptibility is shown in Fig. 3. Agreement with both is excellent; small differences can be seen in the specific heat at higher temperatures, likely due to some uncertainty in the subtraction of the lattice contribution. Comparison to a cut of the INS data at 0.25 K is shown in Fig. 2(a), along with an illustration of the level structure of the single tetrahedron model with the parameters of Eq. (3). The level structure matches very well with the energies of the peaks in the INS cut at 0.25 K. Explicitly one has the spectrum

$$\begin{aligned} E_0 &\equiv 0.000 \text{ meV } (E), & E_{3'} &= 0.754 \text{ meV } (E), \\ E_1 &= 0.382 \text{ meV } (A_2), & E_4 &= 1.802 \text{ meV } (T_2), \\ E_2 &= 0.530 \text{ meV } (T_1), & E_{4'} &= 1.802 \text{ meV } (E), \\ E_3 &= 0.806 \text{ meV } (T_2), \end{aligned} \tag{4}$$

where the irreducible representation in T_d of each level is indicated. We note that the E_4 and $E_{4'}$ levels are very close in energy, but not exactly equal. The model also accurately reproduces the wave vector and temperature dependence of the INS data as can be seen in Fig. 2(c),(d),(f). Additional comparisons to magnetization and INS data can be found in the Supplemental Material [45]. Some of the features of these energy levels can be better understood by adopting global quantization axes and defining global pseudo-spin operators $\tilde{\mathbf{S}}_i$. Using the notation of Ref. [54], the model in the global basis is parametrized by four anisotropic exchanges J_1, J_2, J_3 and J_4. The best fit parameters of Eq. (3) correspond to the values [45]

$$\begin{aligned} J_1 &= +0.587 \text{ meV}, & J_2 &= +0.573 \text{ meV}, \\ J_3 &= -0.011 \text{ meV}, & J_4 &= -0.117 \text{ meV}. \end{aligned} \tag{5}$$

Since $J_1 \sim J_2 \equiv J$ and $J_3 \sim 0$ to a fair approximation, these fitted parameters describe a Heisenberg antiferromagnet supplemented with large (indirect) DM interaction $D \equiv \sqrt{2}J_4 \sim -0.28J$ [45, 55] and negligible symmetric anisotropies. We can thus understand the E doublet ground state as an extension of the pair of $S = 0$ singlets that form the ground state in the Heisenberg limit [33]. Similarly, the approximate quintet $E_4 \sim E_{4'}$ can be mapped to the high energy, five-fold degenerate $S = 2$ states of the antiferromagnetic Heisenberg model. Indeed, when only Heisenberg and DM interactions are present these remain exact eigenstates and degenerate, leaving only the small symmetric anisotropies to provide any splitting. While this mapping is appealing, there are key differences; for example, the three $S = 1$ triplets present in the Heisenberg model are strongly mixed by the DM interactions.

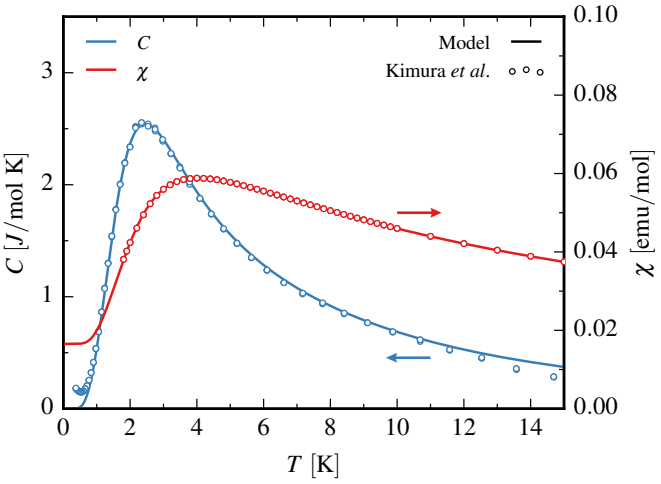

FIG. 3. Comparison of the (magnetic) specific heat, C, and susceptibility, χ, of Kimura *et al.* [33] to the model of Eq. (2) with fitted parameters of Eq. (3). A constant shift χ_0 was included in the fit of the susceptibility to account for the Van Vleck and diamagnetic core contributions of the Yb^{3+} ions.

Discussion: The physics at very low temperatures, $T \ll E_1$, should be primarily controlled by the ground E doublet. The states of this E doublet, $|\pm\rangle$, are rather exotic. As in the Heisenberg limit, they are largely non-magnetic, carrying a uniform (scalar) spin-chirality $\kappa \equiv \langle \tilde{\mathbf{S}}_i \cdot (\tilde{\mathbf{S}}_j \times \tilde{\mathbf{S}}_k) \rangle \sim 0.4$ on each triangle of the tetrahedron [33]. However, due to the large DM interaction, the states additionally acquire all-in/all-out (AIAO) moments. This is generically expected as the AIAO moments and the uniform spin-chirality transform identically under the tetrahedral symmetry [42, 43]. Explicitly, the projection of a pseudo-spin $\mathbf{S}_i$ in the local basis into the E doublet takes the form $\langle \pm | \mathbf{S}_i | \pm \rangle = \pm\lambda\hat{\mathbf{z}}$ with $\lambda \sim 0.13$ for the parameters of Eq. (3) and $\langle \pm | \mathbf{S}_i | \mp \rangle = 0$. These AIAO moments are *octupolar* in character, with the net magnetic moment on each tetrahedron vanishing. Due to the smallness of the inter-tetrahedron interactions we thus expect BYZO to be an octupolar paramagnet at temperatures much smaller than E_1. Direct signatures of this unusual paramagnetic state may appear in more indirect magnetic probes, such as the non-linear susceptibilities.

Going to even lower temperatures one can potentially see indications of collective behavior of the small tetrahedra. Depending on the structure of the inter-tetrahedron interactions, a variety of states could be stabilized, such as weak AIAO order or non-magnetic valence bond solid phases [42, 43]. Tantalizing hints of the onset of such correlations may already be present in the experimental data. We note that the INS data is slightly broader than calculated instrumental resolution (by ~ 0.01 meV) which may be suggestive of weak dispersion, while the specific heat data of Kimura *et al.* [33] shows a slight upturn below ~ 500 mK that is not explained by the single-tetrahedron model. We thus suspect that the current lowest temperatures explored in BYZO are at the threshold of observing such inter-tetrahedron correlations and possibly

even ordering of these E doublet states. Given the complete characterization of the intra-tetrahedron physics presented in this work, we feel the field is well poised to push the study of BYZO to even lower temperatures and explore such inter-tetrahedra physics.

We thank J. Y. Y. Lin for the help with the data reduction. A.D.C., M.D.L. and L.S.W. thank A. Chernyshev, P. Maksimov, G. Ehlers, and I. Zaliznyak for useful discussions. We thank K. Kimura and S. Nakatsuji for kindly providing their data from Ref. [33]. The research at the Spallation Neutron Source (ORNL) is supported by the Scientific User Facilities Division, Office of Basic Energy Sciences, U.S. Department of Energy (DOE). AFM was supported by the U. S. Department of Energy, Office of Science, Basic Energy Sciences, Materials Sciences and Engineering Division. Research supported in part by the Laboratory Directed Research and Development Program of Oak Ridge National Laboratory, managed by UT-Battelle, LLC, for the U. S. Department of Energy. The work at U. of Waterloo was supported by the NSERC of Canada, the Canada Research Chair program (M.J.P.G., Tier 1), the Canadian Foundation for Advanced Research and the Perimeter Institute (PI) for Theoretical Physics. Research at PI is supported by the Government of Canada through Industry Canada and by the Province of Ontario through the Ministry of Economic Development & Innovation.

J.G.R. and L.S.W. contributed equally to this work.

---

† jeff.rau@uwaterloo.ca

‡ wul1@ornl.gov

[1] C. Lacroix, P. Mendels, and F. Mila, eds., *Introduction to Frustrated Magnetism* (Springer Berlin Heidelberg, 2011).

[2] G. Tarjus, S. A. Kivelson, Z. Nussinov, and P. Viot, J. Phys.:Condens. Mat. **17**, R1143 (2005).

[3] G. Watanabe and T. Maruyama, in *Neutron Star Crust*, edited by C. Bertulani and J. Piekarewicz (Nova Science Publishers, New York, 2012) pp. 23–44.

[4] L. Balents, Nature **464**, 199 (2010).

[5] H. T. Diep, *Frustrated Spin Systems* (World Scientific Pub Co Pte Lt, 2013).

[6] P. Santini, S. Carretta, G. Amoretti, R. Caciuffo, N. Magnani, and G. H. Lander, Rev. Mod. Phys. **81**, 807 (2009).

[7] O. A. Starykh, Rep. Prog. Phys. **78**, 052502 (2015).

[8] Y. Iqbal, H. O. Jeschke, J. Reuther, R. Valentí, I. I. Mazin, M. Greiter, and R. Thomale, Phys. Rev. B **92**, 220404 (2015).

[9] B. Fåk, E. Kermarrec, L. Messio, B. Bernu, C. Lhuillier, F. Bert, P. Mendels, B. Koteswararao, F. Bouquet, J. Ollivier, A. D. Hillier, A. Amato, R. H. Colman, and A. S. Wills, Phys. Rev. Lett. **109**, 037208 (2012).

[10] A. Bombardi, L. Paolasini, P. Carretta, J. Rodriguez-Carvajal, P. Millet, and R. Caciuffo, J. Mag. Mag. Mat. **272-276**, E659 (2004).

[11] A. Läuchli, F. Mila, and K. Penc, Phys. Rev. Lett. **97**, 229901 (2006).

[12] M. J. P. Gingras and P. A. McClarty, Rep. Prog. Phys. **77**, 056501 (2014).

[13] H. R. Molavian, M. J. P. Gingras, and B. Canals, Phys. Rev. Lett. **98**, 157204 (2007).

[14] S. Onoda and Y. Tanaka, Phys. Rev. Lett. **105**, 047201 (2010).

[15] K. A. Ross, L. Savary, B. D. Gaulin, and L. Balents, Phys. Rev. X **1**, 021002 (2011).

[16] L. Savary, K. A. Ross, B. D. Gaulin, J. P. C. Ruff, and L. Balents, Phys. Rev. Lett. **109**, 167201 (2012).

[17] M. E. Zhitomirsky, M. V. Gvozdikova, P. C. W. Holdsworth, and R. Moessner, Phys. Rev. Lett. **109**, 077204 (2012).

[18] A. W. C. Wong, Z. Hao, and M. J. P. Gingras, Phys. Rev. B **88**, 144402 (2013).

[19] J. G. Rau, S. Petit, and M. J. P. Gingras, (2015), arXiv:1510.04292 [cond-mat.str-el].

[20] L.-J. Chang, S. Onoda, Y. Su, Y.-J. Kao, K.-D. Tsuei, Y. Yasui, K. Kakurai, and M. R. Lees, Nature Communications **3**, 992 (2012).

[21] J. R. Stewart, G. Ehlers, A. S. Wills, S. T. Bramwell, and J. S. Gardner, J. Phys.:Condens. Mat. **16**, L321 (2004).

[22] J. S. Gardner, S. R. Dunsiger, B. D. Gaulin, M. J. P. Gingras, J. E. Greedan, R. F. Kiefl, M. D. Lumsden, W. A. MacFarlane, N. P. Raju, J. E. Sonier, I. Swainson, and Z. Tun, Phys. Rev. Lett. **82**, 1012 (1999).

[23] K. Kimura, S. Nakatsuji, J.-J. Wen, C. Broholm, M. B. Stone, E. Nishibori, and H. Sawa, Nature Communications **4** (2013), 10.1038/ncomms2914.

[24] K. A. Ross, T. Proffen, H. A. Dabkowska, J. A. Quilliam, L. R. Yaraskavitch, J. B. Kycia, and B. D. Gaulin, Phys. Rev. B **86**, 174424 (2012).

[25] T. Taniguchi, H. Kadowaki, H. Takatsu, B. Fåk, J. Ollivier, T. Yamazaki, T. J. Sato, H. Yoshizawa, Y. Shimura, T. Sakakibara, T. Hong, K. Goto, L. R. Yaraskavitch, and J. B. Kycia, Phys. Rev. B **87**, 060408 (2013).

[26] H. Kadowaki, H. Takatsu, T. Taniguchi, B. Fåk, and J. Ollivier, SPIN **05**, 1540003 (2015).

[27] J. Robert, E. Lhotel, G. Remenyi, S. Sahling, I. Mirebeau, C. Decorse, B. Canals, and S. Petit, Phys. Rev. B **92**, 064425 (2015).

[28] L. D. C. Jaubert, O. Benton, J. G. Rau, J. Oitmaa, R. R. P. Singh, N. Shannon, and M. J. P. Gingras, Phys. Rev. Lett. **115**, 267208 (2015).

[29] N. R. Hayre, K. A. Ross, R. Applegate, T. Lin, R. R. P. Singh, B. D. Gaulin, and M. J. P. Gingras, Phys. Rev. B **87**, 184423 (2013).

[30] J. D. Thompson, P. A. McClarty, H. M. Rønnow, L. P. Regnault, A. Sorge, and M. J. P. Gingras, Phys. Rev. Lett. **106**, 187202 (2011).

[31] R. Applegate, N. R. Hayre, R. R. P. Singh, T. Lin, A. G. R. Day, and M. J. P. Gingras, Phys. Rev. Lett. **109**, 097205 (2012).

[32] J. Oitmaa, R. R. P. Singh, B. Javanparast, A. G. R. Day, B. V. Bagheri, and M. J. P. Gingras, Phys. Rev. B **88**, 220404 (2013).

[33] K. Kimura, S. Nakatsuji, and T. Kimura, Phys. Rev. B **90**, 060414 (2014).

[34] T. Haku, M. Soda, M. Sera, K. Kimura, S. Itoh, T. Yokoo, and T. Masuda, (2015), arXiv:1510.03049 [cond-mat.mtrl-sci].

[35] Y. Okamoto, G. J. Nilsen, J. P. Attfield, and Z. Hiroi, Phys. Rev.

Lett. **110**, 097203 (2013).
[36] Y. Tanaka, M. Yoshida, M. Takigawa, Y. Okamoto, and Z. Hiroi, Phys. Rev. Lett. **113**, 227204 (2014).
[37] Y. Okamoto, G. J. Nilsen, T. Nakazono, and Z. Hiroi, J. Phys. Soc. Jpn. **84**, 043707 (2015).
[38] L. Savary, H.-Y. Kee, Y. B. Kim, and G. Chen, (2015), arXiv:1511.06972 [cond-mat.str-el].
[39] O. Benton and N. Shannon, J. Phys. Soc. Jpn. **84**, 104710 (2015).
[40] H. Tsunetsugu, J. Phys. Soc. Jpn. **70**, 640 (2001).
[41] H. Tsunetsugu, Phys. Rev. B **65**, 024415 (2001).
[42] V. N. Kotov, M. E. Zhitomirsky, M. Elhajal, and F. Mila, Phys. Rev. B **70**, 214401 (2004).
[43] V. N. Kotov, M. E. Zhitomirsky, M. Elhajal, and F. Mila, J. Phys.:Condens. Mat. **16**, S905 (2004).
[44] V. N. Kotov, M. Elhajal, M. E. Zhitomirsky, and F. Mila, Phys. Rev. B **72**, 014421 (2005).
[45] See Supplemental Material at [URL will be inserted by publisher] where we discuss additional details regarding the sample preparation and characterization, the inelastic neutron scattering measurements and the fitting procedure and also includes additional Refs. [S3] and [S6].
[46] A. J. C. Wilson, *International Tables for Crystallography: Mathematical, physical, and chemical tables*, Vol. 3 (International Union of Crystallography, 1992).
[47] A. Huq, J. P. Hodges, L. Heroux, and O. Gourdon, Zeitschrift fur Kristallographie Proceedings **1**, 127 (2011).
[48] M. Scheikowski and H. Müller-Buschbaum, Zeitschrift fr anorganische und allgemeine Chemie **619**, 559 (1993).
[49] C. Rabbow and H. Müller-Buschbaum, Zeitschrift fr anorganische und allgemeine Chemie **622**, 100 (1996).
[50] B. Winn, U. Filges, V. O. Garlea, M. Graves-Brook, M. Hagen, C. Jiang, M. Kenzelmann, L. Passell, S. M. Shapiro, X. Tong, and I. Zaliznyak, in *EPJ Web of Conferences*, Vol. 83 (EDP Sciences, 2015) p. 03017.
[51] J. G. Rau and M. J. P. Gingras, Phys. Rev. B **92**, 144417 (2015).
[52] The case of a dipolar-octupolar doublet ($\Gamma_5 \oplus \Gamma_6$) is in principle possible as well, with a different anisotropic exchange model [56]. We find such a model does not provide a good description of the specific heat or magnetic susceptibility of BYZO and thus consider only an effective spin-1/2 (Γ_4) doublet. This is consistent with the Γ_4 ground doublet found in Ref. [34] by fitting the observed crystal field excitations.
[53] Fitting only the specific heat and susceptibility from Ref. [33] does not produce a unique fit, but many equally good fits. However, these differ significantly when including constraints that arise from fitting the INS data.
[54] H. Yan, O. Benton, L. D. C. Jaubert, and N. Shannon, (2013), arXiv:1311.3501 [cond-mat.str-el].
[55] B. Canals, M. Elhajal, and C. Lacroix, Phys. Rev. B **78**, 214431 (2008).
[56] Y.-P. Huang, G. Chen, and M. Hermele, Phys. Rev. Lett. **112**, 167203 (2014).

Supplemental Material for "Anisotropic exchange within decoupled tetrahedra in the quantum breathing pyrochlore $Ba_3Yb_2Zn_5O_{11}$"*

J. G. Rau,[1,†] L. S. Wu,[2,‡] A. F. May,[3] L. Poudel,[2,4] B. Winn,[2] V. O. Garlea,[2] A. Huq,[5] P. Whitfield,[5] A. E. Taylor,[2] M. D. Lumsden,[2] M. J. P. Gingras,[1,6,7] and A. D. Christianson[2,4]

[1]*Department of Physics and Astronomy, University of Waterloo, Ontario, N2L 3G1, Canada*
[2]*Quantum Condensed Matter Division, Oak Ridge National Laboratory, Oak Ridge, TN-37831, USA*
[3]*Materials Science & Technology Division, Oak Ridge National Laboratory, Oak Ridge, TN-37831, USA*
[4]*Department of Physics & Astronomy, University of Tennessee, Knoxville, TN-37966, USA*
[5]*Chemical & Engineering Materials Division, Oak Ridge National Laboratory, Oak Ridge, TN 37831, USA*
[6]*Perimeter Institute for Theoretical Physics, Waterloo, Ontario, N2L 2Y5, Canada*
[7]*Canadian Institute for Advanced Research, 180 Dundas Street West, Suite 1400, Toronto, ON, M5G 1Z8, Canada*

(Dated: January 16, 2016)

I. SAMPLE SYNTHESIS

Polycrystalline samples of $Ba_3Yb_2Zn_5O_{11}$ were synthesized by solid-state reaction in Al_2O_3 crucibles. The high-purity reactants (dried Yb_2O_3, $BaCO_3$, ZnO) were ground together for 5-10 minutes using an agate milling set in a SPEX SamplePrep Mixer/Mill. The mixture was pressed into pellets, which were initially fired at 1150°C for 25-50 h (in air). Subsequent milling, pellet pressing, and annealing at temperatures up to 1170°C were utilized to promote homogeneity and phase purity in the final product. A slight excess (up to 4 at.%) of Ba and Zn-containing reactants was utilized to minimize the chance of forming Yb-containing impurities.

II. SPECIFIC HEAT AND MAGNETIC SUSCEPTIBILITY

Magnetization measurements were performed upon cooling in an applied field of 0.1 T, and isothermal magnetization measurements were performed at 1.9 K; Quantum Design's Magnetic Property Measurement System was utilized for magnetic measurements. Specific heat measurements were performed in a Quantum Design Physical Property Measurement System.

The specific heat of $Ba_3Yb_2Zn_5O_{11}$ is shown in Fig. S1. The specific heat of a sample from the same batch used for the inelastic neutron scattering measurements is compared with that from Kimura *et al.* [S1]. Both measurements are consistent with a maximum at ~ 2.4 K.

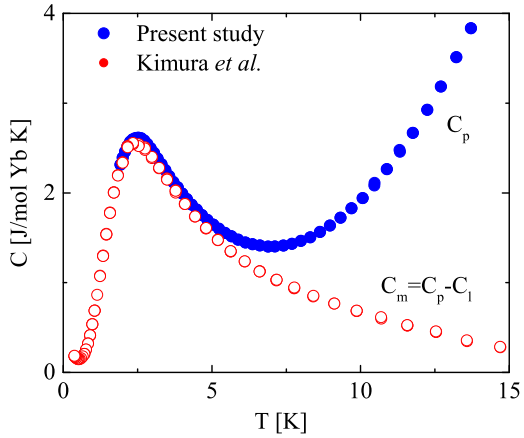

FIG. S1. The temperature dependent specific heat of $Ba_3Yb_2Zn_5O_{11}$. Filled circles are from measurements of a piece taken from the same batch as used for the inelastic neutron scattering measurements. Open circles are the magnetic contribution to the specific heat (C_m) taken from Kimura *et al.* [S1], determined C_m by subtracting the lattice contribution (C_l) estimated from $Ba_3Lu_2Zn_5O_{11}$ from the specific heat of $Ba_3Yb_2Zn_5O_{11}$ (C_p).

The magnetic susceptibility and inverse susceptibility of a sample taken from the same batch as the sample used for the inelastic neutron scattering data are shown in Fig. S2 for an applied field of 0.1 T. A maximum in the susceptibility occurs at ~ 4 K.

III. NEUTRON DIFFRACTION

Neutron powder diffraction measurements of $Ba_3Yb_2Zn_5O_{11}$ were performed with the time-of-flight powder diffractometer POWGEN, at the Spallation Neutron Source (SNS) at Oak Ridge National Laboratory [S2]. Data were collected on a powder $Ba_3Yb_2Zn_5O_{11}$ sample with mass 6.32 g. The data were collected for 2 hours at temperatures 10 K and 300 K, respectively. Structural refinement was carried out using the software package FULLPROF [S3]

* This manuscript has been authored by UT-Battelle, LLC under Contract No. DE-AC05-00OR22725 with the U.S. Department of Energy. The United States Government retains and the publisher, by accepting the article for publication, acknowledges that the United States Government retains a non-exclusive, paid-up, irrevocable, world-wide license to publish or reproduce the published form of this manuscript, or allow others to do so, for United States Government purposes. The Department of Energy will provide public access to these results of federally sponsored research in accordance with the DOE Public Access Plan (http://energy.gov/downloads/doe-public-access-plan).

† jeff.rau@uwaterloo.ca
‡ wul1@ornl.gov

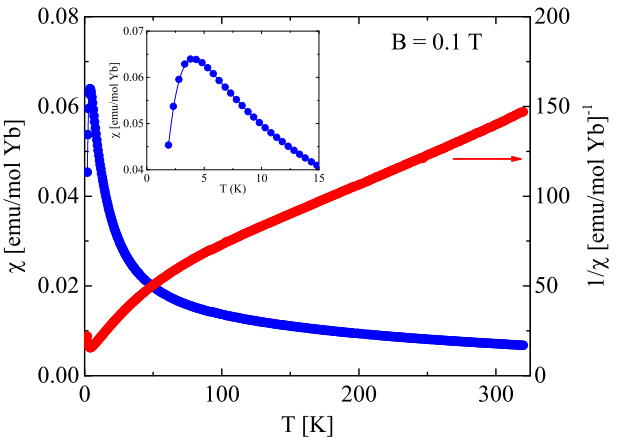

FIG. S2. Left axis: The temperature dependent static magnetic susceptibility ($\chi = M/B$) for $Ba_3Yb_2Zn_5O_{11}$ (blue circles), measured in field $B = 0.1$ T from temperature 1.9 to 320 K. Right axis: The inverse magnetic susceptibility ($1/\chi$) as a function of temperature. The inset shows an expanded view of the low temperature region, where a maximum in the susceptibility occurs around 4 K.

Atom	Wyckoff	x	y	z	B_{iso}	Occ.
Ba	24f	0.7055(3)	0.00000	0.00000	0.1313(0)	0.25000
Yb	16e	0.8365(5)	0.8365(5)	0.8365(5)	0.1187(9)	0.16670
Zn(1)	16e	0.0832(5)	0.0832(5)	0.0832(5)	0.1155(4)	0.16670
Zn(2)	24g	0.25000	0.25000	0.0828(1)	0.1729(2)	0.25000
O(1)	4b	0.50000	0.50000	0.50000	0.4219(9)	0.04167
O(2)	4a	0.00000	0.00000	0.00000	0.2334(2)	0.04167
O(3)	16e	0.3419(3)	0.3419(3)	0.3419(3)	0.3313(9)	0.16670
O(4)	16e	0.6679(6)	0.6679(6)	0.6679(6)	0.3777(2)	0.16670
O(5)	48h	0.1660(2)	0.1660(2)	1.0000(4)	0.30015(0)	0.50000

Atom	Wyckoff	x	y	z	B_{iso}	Occ.
Ba	24f	0.7055(6)	0.00000	0.00000	0.7268(4)	0.25000
Yb	16e	0.8365(5)	0.8365(5)	0.8365(5)	0.4480(3)	0.16670
Zn(1)	16e	0.0832(9)	0.0832(9)	0.0832(9)	0.4184(2)	0.16670
Zn(2)	24g	0.25000	0.25000	0.0824(7)	0.5697(8)	0.25000
O(1)	4b	0.50000	0.50000	0.50000	0.8089(3)	0.04167
O(2)	4a	0.00000	0.00000	0.00000	0.4878(2)	0.04167
O(3)	16e	0.3421(4)	0.3421(4)	0.3421(4)	0.6450(5)	0.16670
O(4)	16e	0.6683(0)	0.6683(0)	0.6683(0)	0.7374(4)	0.16670
O(5)	48h	0.1659(4)	0.1659(4)	1.0001(6)	0.6505(3)	0.50000

TABLE S1. Atomic parameters for $Ba_3Yb_2Zn_5O_{11}$ at 10 K (top panel) and 300 K (bottom panel).

The neutron diffraction data at 10 and 300 K along with the Rietveld refinement of the structural model is shown in Fig. S3(a) and (b) respectively. The fitted model describes the data well over a wide wave vector range ($1.3 < |\mathbf{Q}| < 21$ Å^{-1}). A few unindexed impurity peaks with intensities less than 1% of the main diffraction peaks of $Ba_3Yb_2Zn_5O_{11}$ are observed. The small fraction of impurities appears to be consistent with that found by Kimura *et al.* [S1] and indicates that the sample consists primarily of the cubic $Ba_3Yb_2Zn_5O_{11}$ phase. No site vacancies or disorder between sites was detected within

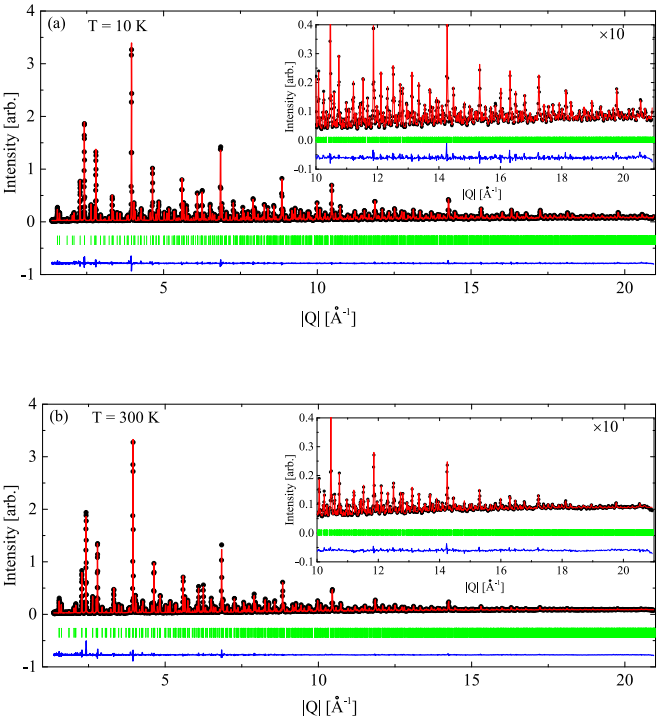

FIG. S3. Neutron powder diffraction data collected with POWGEN at 10 K (a) and 300 K (b) for $Ba_3Yb_2Zn_5O_{11}$. Rietveld refinement (red line), difference pattern (blue line) and calculated reflection positions (green ticks) are superimposed on the data points (black circles). The insets show an expanded view of the high $|\mathbf{Q}|$ region of the data.

T (K)	a (Å)	R_p	R_{wp}	R_{exp}	χ^2
10	13.47117(3)	9.07	8.63	1.53	31.8
300	13.48997(3)	10.7	9.23	1.99	21.5

TABLE S2. Comparison of the refinement parameters at 10 and 300 K.

experimental resolution. The refined atomic parameters of $Ba_3Yb_2Zn_5O_{11}$ at 10 K and 300 K are shown in Table S1. The lattice constants and goodness of fit parameters are displayed in Table S2.

IV. INELASTIC NEUTRON SCATTERING

Inelastic neutron scattering (INS) experiments were performed on the hybrid spectrometer (HYSPEC) at the Spallation Neutron Source at Oak Ridge National Laboratory [S5]. The data were collected at 0.25 K, 10 K, and 20 K utilizing a ^{3}He refrigerator, with incident energies $E_i = 3.8$, 7.5, and 15 meV and Fermi chopper frequencies of 180, 300, and 300 Hz respectively. To cover a large region of reciprocal space the center of the detector vessel, which covers 60° of scattering angle, was placed at scattering angles ranging from 33 - 101°.

Shown in Fig. S4(a), and Fig. S4(b) are the intensity maps of the inelastic neutron scattering data of $Ba_3Yb_2Zn_5O_{11}$ with $E_i = 15$ meV measured at temperatures 0.25 K and 10 K.

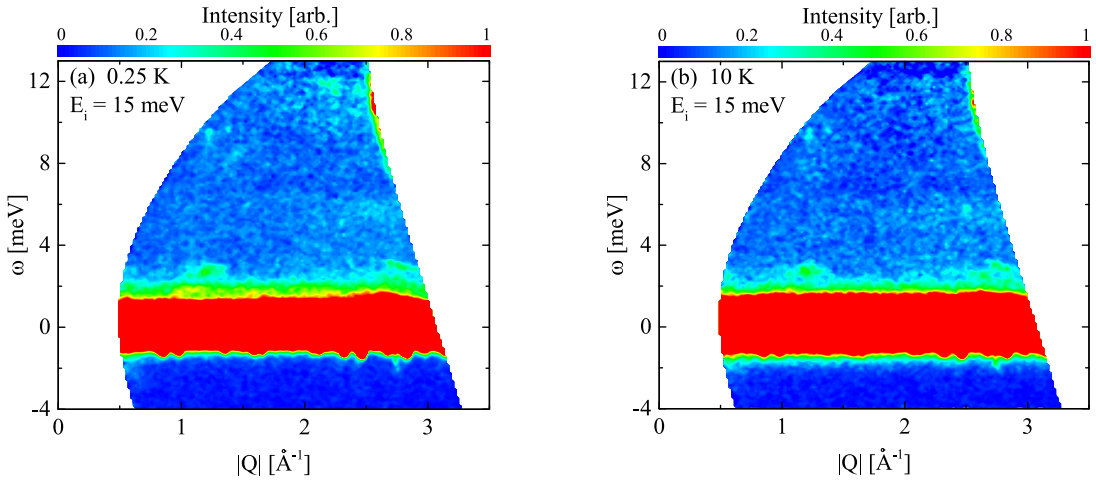

FIG. S4. Intensity map of the inelastic neutron scattering from $Ba_3Yb_2Zn_5O_{11}$ with E_i = 15 meV at 0.25 K (a) and 10 K (b).

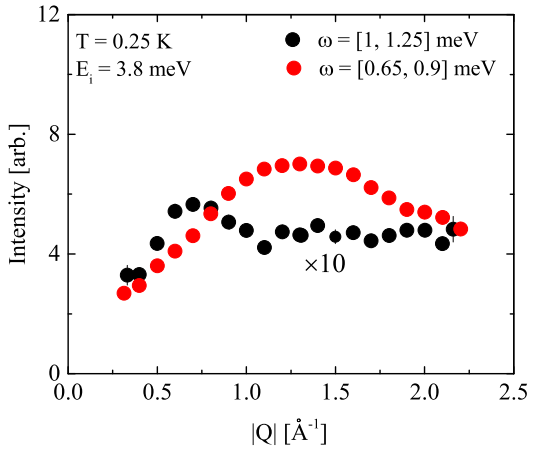

FIG. S5. Wave vector |**Q**| dependent neutron scattering intensity measured at 0.25 K with incident energy E_i = 3.8 meV, averaged over the excitation energy window $\omega = [0.65, 0.9]$ meV (red points) and $\omega = [1, 1.25]$ meV (black points).

Although the low energy excitations are not well resolved with E_i = 15 meV, the data shown in Fig. S4 confirm that there is no additional excitations up to 13.75 meV, which is consistent with the model described in the main text.

As mentioned in the main text, we noticed that there is a weak broad feature in the INS spectrum near an energy transfer of 1 meV (main text Fig. 2(a)). However, this feature has a significantly different dependence on wave vector |**Q**| from that of the other observed modes. Fig. S5 shows the wave vector |**Q**| dependent neutron scattering intensity measured at 0.25 K with incident energy E_i = 3.8 meV, averaged over the excitation energy window $\omega = [0.65, 0.9]$ meV and $\omega = [1, 1.25]$ meV. In contrast to the well defined inelastic mode contained in the energy range $\omega = [0.65, 0.9]$ meV, which peaks near $|\mathbf{Q}| = 1.3\text{Å}^{-1}$, the broad feature captured by the integration range, $\omega = [1, 1.25]$ meV is much weaker with a small peak around $|\mathbf{Q}| = 0.7\text{Å}^{-1}$.

As a supplement to the data collected at 0.25 K and 20 K with E_i = 3.8 meV described and shown in the main text, data collected with E_i = 3.8 meV at 10 K is shown in Fig. S6 below. The HYSPEC instrumental energy resolution with E_i = 3.8 meV and the 180 Hz chopper setting used experimentally is shown in Fig. S7 as a function of energy transfer. The |**Q**| dependence of the inelastic spectrum is shown through a series of cuts with an energy range of [0.65, 0.9] meV at temperatures of 0.25, 10, and 20 K in Fig. S8.

V. CRYSTAL FIELD EXCITATIONS

Inelastic neutron scattering data was collected with the ARCS [S6] time-of-flight spectrometer to probe the excitation spectrum at higher energies. This data was collected at 10 K with E_i = 100 meV and shows three crystal field excitations at ~ 38, 54, and 67 meV. The data presented here are consistent with the results of Ref. [S7] where a more detailed analysis of the crystal field excitation spectrum and Hamiltonian can be found. We note that for a Kramers ion such as Yb^{3+} ($J = 7/2$), in the absence of broken time reversal symmetry, the minimum degeneracy is two so that $(2J+1)/2$ doublets are expected including the ground state. Thus the observation of three crystal field excitations is strong evidence that the modes observed at energies less than ~ 2 meV discussed in the main paper are due to interactions between the Yb^{3+} within each tetrahedron.

VI. THEORETICAL DETAILS

A. Model

For completeness, we state our model and conventions in more detail. We consider the effective anistoropic exchange

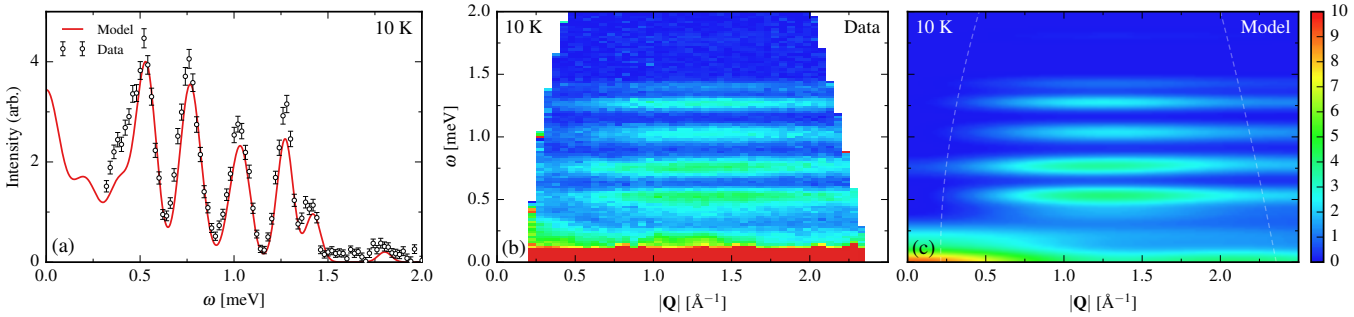

FIG. S6. Inelastic neutron scattering data (E_i=3.8 meV) and comparison to theoretical model at (a-c) 10 K. The overall theoretical intensity scale was fit using the INS cut at 0.25 K. A Gaussian broadening with energy dependence following the experimental energy resolution function (shown in Fig. S7) was included in the theoretical calculation. (a) Cut of INS data averaged over the window 1.25Å^{-1} < |**Q**| < 1.35Å^{-1}. Results for the best fit single tetrahedron model of the main text are shown. (b) Intensity map of powder averaged INS data. The excitations are nearly dispersion free over the full |**Q**| range. (c) Model calculations for the best fit single tetrahedron model. The Yb^{3+} form factor was evaluated in the dipole approximation, as given in Ref. [S4].

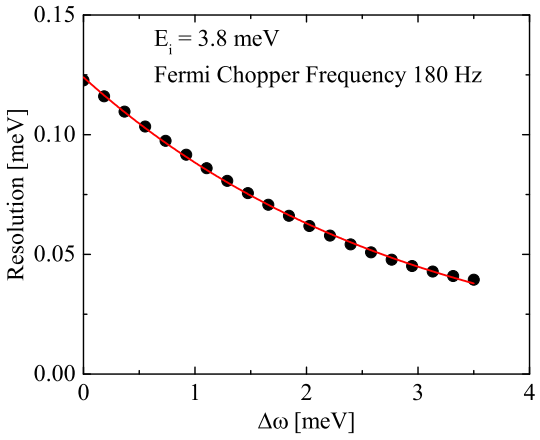

FIG. S7. HYSPEC resolution as a function of the energy transfer $\Delta\omega$, with incident energy E_i = 3.8 meV and Fermi chopper frequency of 180 Hz. The red line is the fit to the empirical equation $y = Ae^{-\Delta\omega/\Gamma}$ with A = 0.12398 ± 0.0004 meV, and Γ = 2.95111 ± 0.02144 meV.

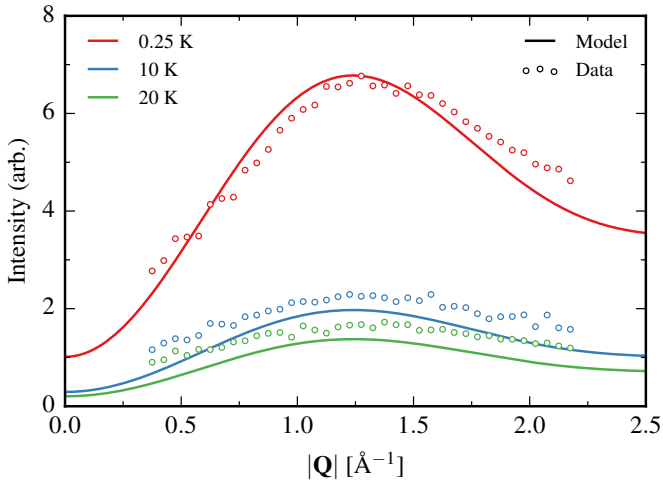

FIG. S8. The |**Q**| dependence of the inelastic neutron scattering data for $Ba_3Yb_2Zn_5O_{11}$, averaged over the excitation in the energy window 0.65 meV < ω < 0.9 meV.

model in the local basis defined as

$$H_{\text{eff}} \equiv \sum_{i=1}^{4}\sum_{j<i}\Big[J_{zz}S_i^zS_j^z - J_\pm\left(S_i^+S_j^- + S_i^-S_j^+\right) + J_{\pm\pm}\left(\gamma_{ij}S_i^+S_j^+ + \text{h.c}\right) + J_{z\pm}\left(\zeta_{ij}\left[S_i^zS_j^+ + S_i^+S_j^z\right] + \text{h.c}\right)\Big] - \mu_B\mathbf{B}\cdot\sum_{i=1}^{4}\left[g_\pm\left(\hat{\mathbf{x}}_iS_i^x + \hat{\mathbf{y}}_iS_i^y\right) + g_z\hat{\mathbf{z}}_iS_i^z\right], \quad \text{(S1)}$$

with four symmetry allowed exchanges J_{zz}, $J_\pm$, $J_{\pm\pm}$ and $J_{z\pm}$ and external magnetic field **B**. The complex bond phase factors γ_{ij} and $\zeta_{ij} = -\gamma_{ij}^*$ depend only on the basis sites they connect and thus can be expressed as a matrix

$$\gamma = \begin{pmatrix} 0 & +1 & \omega & \omega^2 \\ +1 & 0 & \omega^2 & \omega \\ \omega & \omega^2 & 0 & +1 \\ \omega^2 & \omega & +1 & 0 \end{pmatrix}, \quad \text{(S2)}$$

where $\omega = e^{2\pi i/3}$. The magnetic field is coupled directly to the effective moment on each Yb^{3+} site, defined as

$$\boldsymbol{\mu}_i \equiv \mu_B\left[g_\pm\left(\hat{\mathbf{x}}_iS_i^x + \hat{\mathbf{y}}_iS_i^y\right) + g_z\hat{\mathbf{z}}_iS_i^z\right], \quad \text{(S3)}$$

where g_z and $g_\pm$ are the g-factors in the local [111] direction and in the plane perpendicular to it. These local axes are de-

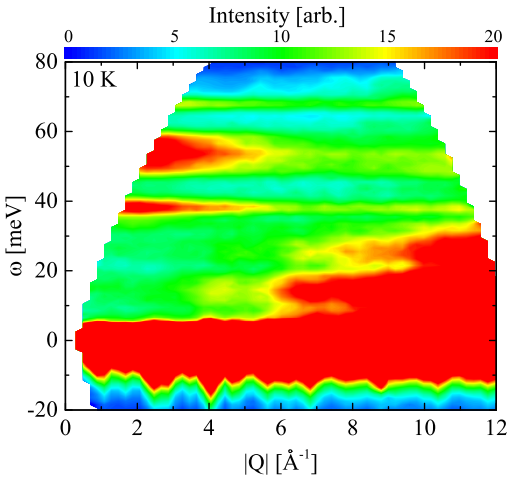

FIG. S9. Intensity map of the inelastic neutron scattering data from $Ba_3Yb_2Zn_5O_{11}$ with $E_i = 100$ meV at 10 K . The data shows three crystal field excitations at 38, 54, and 67 meV.

fined as

$$\begin{aligned}
\hat{\mathbf{z}}_1 &= \frac{1}{\sqrt{3}}(+\hat{\mathbf{x}}+\hat{\mathbf{y}}+\hat{\mathbf{z}}), \quad \hat{\mathbf{x}}_1 = \frac{1}{\sqrt{6}}(-2\hat{\mathbf{x}}+\hat{\mathbf{y}}+\hat{\mathbf{z}}),\\
\hat{\mathbf{z}}_2 &= \frac{1}{\sqrt{3}}(+\hat{\mathbf{x}}-\hat{\mathbf{y}}-\hat{\mathbf{z}}), \quad \hat{\mathbf{x}}_2 = \frac{1}{\sqrt{6}}(-2\hat{\mathbf{x}}-\hat{\mathbf{y}}-\hat{\mathbf{z}}),\\
\hat{\mathbf{z}}_3 &= \frac{1}{\sqrt{3}}(-\hat{\mathbf{x}}+\hat{\mathbf{y}}-\hat{\mathbf{z}}), \quad \hat{\mathbf{x}}_3 = \frac{1}{\sqrt{6}}(+2\hat{\mathbf{x}}+\hat{\mathbf{y}}-\hat{\mathbf{z}}),\\
\hat{\mathbf{z}}_4 &= \frac{1}{\sqrt{3}}(-\hat{\mathbf{x}}-\hat{\mathbf{y}}+\hat{\mathbf{z}}), \quad \hat{\mathbf{x}}_4 = \frac{1}{\sqrt{6}}(+2\hat{\mathbf{x}}-\hat{\mathbf{y}}+\hat{\mathbf{z}}),
\end{aligned} \tag{S4}$$

where $\hat{\mathbf{y}}_i = \hat{\mathbf{z}}_i \times \hat{\mathbf{x}}_i$.

Equivalently, this model can be expressed in *global* quantization axes [S8]. We thus define a global pseudo-spin operator $\tilde{\mathbf{S}}_i$ for each Yb^{3+} site as

$$\tilde{\mathbf{S}}_i \equiv \hat{\mathbf{x}}_i S_i^x + \hat{\mathbf{y}}_i S_i^y + \hat{\mathbf{z}}_i S_i^z. \tag{S5}$$

In this basis the anisotropic exchange model can be written

$$H_{\text{eff}} \equiv \sum_{j=1}^{4}\sum_{i<j} \tilde{\mathbf{S}}_i^{\intercal} \mathbf{J}_{ij} \tilde{\mathbf{S}}_j, \tag{S6}$$

where the exchange matrices $\mathbf{J}_{ij}$ are defined as

$$\begin{aligned}
\mathbf{J}_{12} &= \begin{pmatrix} J_2 & J_4 & J_4 \\ -J_4 & J_1 & J_3 \\ -J_4 & J_3 & J_1 \end{pmatrix}, \quad \mathbf{J}_{13} = \begin{pmatrix} J_1 & -J_4 & J_3 \\ J_4 & J_2 & J_4 \\ J_3 & -J_4 & J_1 \end{pmatrix},\\
\mathbf{J}_{14} &= \begin{pmatrix} J_1 & J_3 & -J_4 \\ J_3 & J_1 & -J_4 \\ J_4 & J_4 & J_2 \end{pmatrix}, \quad \mathbf{J}_{23} = \begin{pmatrix} J_1 & -J_3 & J_4 \\ -J_3 & J_1 & -J_4 \\ -J_4 & J_4 & J_2 \end{pmatrix},\\
\mathbf{J}_{24} &= \begin{pmatrix} J_1 & J_4 & -J_3 \\ -J_4 & J_2 & J_4 \\ -J_3 & -J_4 & J_1 \end{pmatrix}, \quad \mathbf{J}_{34} = \begin{pmatrix} J_2 & -J_4 & J_4 \\ J_4 & J_1 & -J_3 \\ -J_4 & -J_3 & J_1 \end{pmatrix}.
\end{aligned} \tag{S7}$$

These two different parametrizations are related as

$$\begin{aligned}
J_1 &= \frac{1}{3}\left(+4J_\pm + 2J_{\pm\pm} + 2\sqrt{2}J_{z\pm} - J_{zz}\right),\\
J_2 &= \frac{1}{3}\left(-4J_\pm + 4J_{\pm\pm} + 4\sqrt{2}J_{z\pm} + J_{zz}\right),\\
J_3 &= \frac{1}{3}\left(-2J_\pm - 4J_{\pm\pm} + 2\sqrt{2}J_{z\pm} - J_{zz}\right),\\
J_4 &= \frac{1}{3}\left(-2J_\pm + 2J_{\pm\pm} - \sqrt{2}J_{z\pm} - J_{zz}\right).
\end{aligned} \tag{S8}$$

As discussed in the main text, the exchange J_4 can be interpreted as a Dzyaloshinskii-Moriya (DM) interaction. Specifically, for $J_1 = J_2 \equiv J$ and $J_3 = 0$ we can write

$$H_{\text{eff}} = \sum_{j=1}^{4}\sum_{i<j}\left[J\tilde{\mathbf{S}}_i \cdot \tilde{\mathbf{S}}_j + \mathbf{D}_{ij} \cdot \left(\tilde{\mathbf{S}}_i \times \tilde{\mathbf{S}}_j\right)\right], \tag{S9}$$

where the DM vectors are defined as $\mathbf{D}_{ij} \equiv D\hat{\mathbf{D}}_{ij}$ with magnitude $D = \sqrt{2}J_4$ and directions

$$\begin{aligned}
\hat{\mathbf{D}}_{12} &= \frac{-\hat{\mathbf{y}}+\hat{\mathbf{z}}}{\sqrt{2}}, \quad \hat{\mathbf{D}}_{13} = \frac{+\hat{\mathbf{x}}-\hat{\mathbf{z}}}{\sqrt{2}}, \quad \hat{\mathbf{D}}_{14} = \frac{-\hat{\mathbf{x}}+\hat{\mathbf{y}}}{\sqrt{2}},\\
\hat{\mathbf{D}}_{23} &= \frac{-\hat{\mathbf{x}}-\hat{\mathbf{y}}}{\sqrt{2}}, \quad \hat{\mathbf{D}}_{24} = \frac{+\hat{\mathbf{x}}+\hat{\mathbf{z}}}{\sqrt{2}}, \quad \hat{\mathbf{D}}_{34} = \frac{-\hat{\mathbf{y}}-\hat{\mathbf{z}}}{\sqrt{2}}.
\end{aligned} \tag{S10}$$

With these definitions $J_4 > 0$ corresponds to the so-called direct case, while $J_4 < 0$ corresponds to the indirect case [S9].

B. Observables

The effective single tetrahedron model can be numerically diagonalized exactly and all observable quantities can be directly computed. Below we outline how each observable is computed and compared with the respective experimental results.

1. *Specific heat*

As the lattice contribution has been subtracted in Ref. [S1] using the structural analog $Ba_3Lu_2Zn_5O_{11}$, we simply compute the magnetic contribution directly from the model. This is straightforwardly

$$C = \frac{1}{4}\left(\frac{\langle H_{\text{eff}}^2\rangle - \langle H_{\text{eff}}\rangle^2}{k_B T^2}\right), \tag{S11}$$

where $\langle O\rangle = \text{tr}[Oe^{-\beta H_{\text{eff}}}]/\text{tr}[e^{-\beta H_{\text{eff}}}]$ denotes a thermal average. While the lattice subtraction seems robust, we only use the specific heat data of Kimura *et al.* [S1] below $T < 5$ K to minimize any possible bias from this procedure.

2. *Susceptibility*

We compute the magnetic susceptibility by emulating the experimental procedure of Kimura *et al.* [S1]. We thus add

a small magnetic field with $|\mathbf{B}| = 0.1$ T and the compute magnetization, $\boldsymbol{\mu} \equiv 1/4 \sum_{i=1}^{4} \boldsymbol{\mu}_i$, in the effective single tetrahedron model. To better compare to the experimental results, we need to include Van Vleck contributions from the higher crystal field levels and the diamagnetic susceptibility from the Yb^{3+} core electrons. At these low temperatures, we treat this as a constant shift χ_0 to be added to χ. Estimates from Ref. [S1] place these contributions at roughly $\chi_0 \sim 6.9 \cdot 10^{-3}$ emu/(mol Yb), though we leave χ_0 as a free parameter in our analysis. As we will see below, the fitted value of χ_0 agrees well with this theoretical estimate. In total the susceptibility, χ, is given by

$$\chi \equiv \mu_0 |\langle \boldsymbol{\mu} \rangle| / |\mathbf{B}| + \chi_0, \tag{S12}$$

where $\langle \boldsymbol{\mu} \rangle$ is the magnetization computed in the effective single tetrahedron model in the presence of the magnetic field $\mathbf{B}$. Due to the cubic symmetry, the susceptibility is isotropic and thus the direction $\hat{\mathbf{B}}$ of this applied field is unimportant. We have verified that this field is well within the linear regime, with essentially no difference in computing χ with an extremely small field of $|\mathbf{B}| = 10^{-3}$ T rather than $|\mathbf{B}| = 0.1$ T.

3. *Magnetization*

To compare to the magnetization data of Kimura *et al.* [S1] at larger fields, we compute the magnetization itself as a function of field. As in computing the susceptibility, the χ_0 shift contributes a linear correction to magnetization computed directly from the single tetrahedron model. Explicitly, the total magnetization $\mathbf{M}$ per Yb^{3+} is given as

$$\mathbf{M} \equiv \langle \boldsymbol{\mu} \rangle + \chi_0 \mathbf{B} / \mu_0, \tag{S13}$$

where $\langle \boldsymbol{\mu} \rangle$ is the magnetization computed in the effective single tetrahedron model. Unlike when computing the susceptibility, the magnetization measurements of Ref. [S1] go beyond the linear regime and thus $\langle \boldsymbol{\mu} \rangle$ *does* depend on the field direction $\hat{\mathbf{B}}$. To emulate the inherent averaging in the powder samples, we consider fields with arbitrary direction $\hat{\mathbf{B}}$ and fixed magnitude $|\mathbf{B}|$. For each $\mathbf{B}$ we then compute $\hat{\mathbf{B}} \cdot \mathbf{M}$ and integrate over field directions $\hat{\mathbf{B}}$ to obtain the contribution to the powder averaged magnetization.

4. *Inelastic neutron scattering*

The inelastic neutron scattering intensity is given by

$$I(\mathbf{Q}, \omega) = I_0 \frac{|\mathbf{k}'|}{|\mathbf{k}|} \sum_{\alpha\beta} \left(\delta_{\alpha\beta} - \hat{Q}_\alpha \hat{Q}_\beta \right) F(|\mathbf{Q}|)^2 \mathcal{S}^{\alpha\beta}(\mathbf{Q}, \omega), \tag{S14}$$

where $\mathbf{k}$, $\mathbf{k}'$ are the initial and final neutron momenta, $F(Q)$ is the form factor for Yb^{3+} [S4] and I_0 is a normalization factor. The dynamical structure factor for a single tetrahedron, $\mathcal{S}^{\alpha\beta}(\mathbf{Q}, \omega)$, is given as

$$\mathcal{S}^{\alpha\beta}(\mathbf{Q}, \omega) = \sum_{nn'} \frac{e^{-\beta E_n}}{Z} \langle n | \mu^{\alpha}_{-\mathbf{Q}} | n' \rangle \langle n' | \mu^{\beta}_{\mathbf{Q}} | n \rangle \, \delta(\omega - E_{n'} + E_n),$$

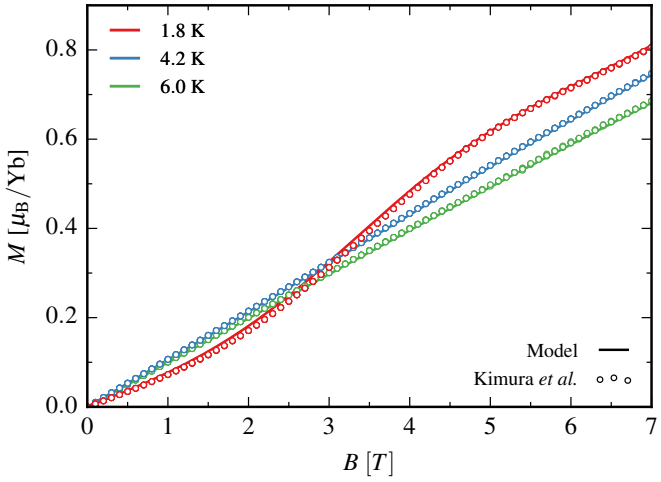

FIG. S10. Comparison of the magnetization data of Kimura *et al.* [S1] at $T = 1.8$ K, 4.2 K and 6.0 K to the model calculations for the best fit parameters. The Van Vleck and core diamagnetic contributions, χ_0, fitted in the susceptibility also contribute to the magnetization.

where $|n\rangle$, E_n are the eigenstates and energies of the single tetrahedron model H_{eff} and Z is the partition function. The operators $\boldsymbol{\mu}_{\mathbf{Q}}$ are defined as

$$\boldsymbol{\mu}_{\mathbf{Q}} \equiv \frac{1}{4} \sum_{i=1}^{4} e^{-i\mathbf{Q}\cdot\mathbf{r}_i} \boldsymbol{\mu}_i, \tag{S15}$$

where $\boldsymbol{\mu}_i$ and $\mathbf{r}_i$ are the Yb^{3+} moments and site positions. The prefactor $|\mathbf{k}'|/|\mathbf{k}| = (1 - \omega/E_{\text{i}})^{1/2}$ and reduces the relative intensity of some higher lying features. For the INS data we are interested in, one has $E_{\text{i}} = 3.8$ meV and this only is significant at high energies. We consider the powder averaged cross section

$$I_{\text{avg}}(Q, \omega) \equiv \int d\hat{\mathbf{Q}} \, I(Q\hat{\mathbf{Q}}, \omega). \tag{S16}$$

Due to the isolated tetrahedra, strictly $I_{\text{avg}}(Q, \omega)$ has features flat in $|\mathbf{Q}|$, and sharp in energy. At low temperature, these simply reflect transitions from the ground state to the excited levels. Additional information resides in the intensity variations. To compare with the experimental data, we include an overall scale factor, I_0, to represent the arbitrary experimental intensity scale. To emulate the finite experimental energy resolution, we convolve $I_{\text{avg}}(Q, \omega)$ with Gaussians of finite width. The experimental energy resolution is energy dependent, varying approximately as $\sim A e^{-\omega/\Gamma}$ as given in Fig. S7. To incorporate this, the width of this Gaussian broadening made energy dependent as well, following this experimental form. However, as the observed levels are somewhat broader than the experimental limit, we allow the overall scale of this energy dependent width, denoted as $A^{(\text{fit})}$, to vary in the theoretical calculation while keeping the experimentally determined value for Γ.

C. Fitting

As discussed in the main text, to fit the experimental data we use the specific heat, susceptibility and a cut of inelastic neutron scattering data averaged over the range $1.25\text{Å}^{-1} < |\mathbf{Q}| < 1.35\text{Å}^{-1}$. Here we present explicit details of our fitting methodology. We denote the specific heat data of Kimura *et al.* [S1] as a set of temperatures $T_n^{(\text{exp},C)}$ and values $C_n^{(\text{exp})}$ where n labels each data point. As discussed in the main text, we only use data points with $T < 5$ K to minimize possible issues with the lattice subtraction. Similarly for the susceptibility, we define $T_n^{(\text{exp},\chi)}$ and $\chi_n^{(\text{exp})}$ (taking all points with $T < 30$ K) and for the INS cut $\omega_n^{(\text{exp},\chi)}$ and $I_n^{(\text{exp})}$ (taking all points with $0.25\text{ meV} < \omega < 2\text{ meV}$ in the $T = 0.25$ K cut). For each temperature T or energy ω we can compute the theoretical values, yielding $C_n^{(\text{theo})}$, $\chi_n^{(\text{theo})}$ and $I_n^{(\text{theo})}$ as outlined in the previous section. Thinking of these sets of observations and theoretical values as vectors, we define the discrepancy

$$\epsilon_X \equiv |\mathbf{X}^{(\text{exp})} - \mathbf{X}^{(\text{theo})}|/|\mathbf{X}^{(\text{exp})}|, \tag{S17}$$

where $X = C, \chi$ or I. To find the best fit of the experimental data, we minimize the sum of these differences $\epsilon_{\text{tot}} \equiv \epsilon_C + \epsilon_\chi + \epsilon_I$. In total we have nine fitting parameters:

1. The exchanges J_{zz}, $J_\pm$, $J_{\pm\pm}$ and $J_{z\pm}$
2. The g-factors, g_z and $g_\pm$
3. The susceptibility shift χ_0
4. The intensity scale of the INS spectrum I_0 and the scale of the Gaussian energy broadening $A^{(\text{fit})}$

We used standard minimization algorithms to find the best fit presented in the main text. To aid in finding the global minimum, the minimization process was repeated for several thousand random initial conditions. To be specific regarding the initialization, the four exchanges were drawn from uniform distributions covering the range $[-0.3, +0.3]$ meV, each g-factor from the range $[1, 3]$ and χ_0 susceptibility shift from the range $[6, 8] \cdot 10^{-3}$ emu/(mol Yb). The neutron intensity was always initialized to $I_0 = 0.01$, while the energy width $A^{(\text{fit})}$ was initialized with the experimental value $A = 0.124$ meV. In the main text, we reported the exchanges and g-factors. The remaining parameters for the best fit are given as

$$I_0 = 0.012, \quad A^{(\text{fit})}/A = 1.24, \quad \chi_0 = 6.75 \cdot 10^{-3}\text{ emu/(mol Yb)}.$$

We see that the susceptibility shift χ_0 compares favorably with the expected theoretical value [S1]. We note that the required scale to the energy broadening is somewhat larger than the experimental resolution, by about 25%, as can be seen directly in the INS cuts at 0.25 K. Additional comparisons of the experimental results and the theoretical model are shown in Fig. S6 (INS at 10 K), Fig. S10 (magnetization) and Fig. S8 ($|\mathbf{Q}|$ dependence of INS intensity).

While the best fit parameters found are qualitatively unique, they can vary somewhat if one changes details of the fitting procedure. For example, by changing temperature ranges used in C or χ, or assigning different relative weights to each data set. The most sensitive of the parameters is J_{zz}, which can vary by as much as 0.02 to 0.04 meV, while the other parameters can vary by 10% or so. None of these variations change the qualitative picture that emerges from our analysis; in the global basis the system predominantly antiferromagnetic Heisenberg and (indirect) DM interactions and small symmetric anisotropies.

[S1] K. Kimura, S. Nakatsuji, and T. Kimura, Phys. Rev. B **90**, 060414 (2014).

[S2] A. Huq, J. P. Hodges, L. Heroux, and O. Gourdon, Zeitschrift fur Kristallographie Proceedings **1**, 127 (2011).

[S3] J. Rodriguez-Carvajal, Physica B: Condensed Matter **192**, 55 (1993).

[S4] A. J. C. Wilson, *International Tables for Crystallography: Mathematical, physical, and chemical tables*, Vol. 3 (International Union of Crystallography, 1992).

[S5] B. Winn, U. Filges, V. O. Garlea, M. Graves-Brook, M. Hagen, C. Jiang, M. Kenzelmann, L. Passell, S. M. Shapiro, X. Tong, and I. Zaliznyak, in *EPJ Web of Conferences*, Vol. 83 (EDP Sciences, 2015) p. 03017.

[S6] D. L. Abernathy, M. B. Stone, M. J. Loguillo, M. S. Lucas, O. Delaire, X. Tang, J. Y. Y. Lin, and B. Fultz, Review of Scientific Instruments **83**, 015114 (2012).

[S7] T. Haku, M. Soda, M. Sera, K. Kimura, S. Itoh, T. Yokoo, and T. Masuda, (2015), arXiv:1510.03049 [cond-mat.mtrl-sci].

[S8] H. Yan, O. Benton, L. D. C. Jaubert, and N. Shannon, (2013), arXiv:1311.3501 [cond-mat.str-el].

[S9] B. Canals, M. Elhajal, and C. Lacroix, Phys. Rev. B **78**, 214431 (2008).